





Magnetogenesis via the canonical battery effect

Modhuchandra Laishram ¹, Gunsu S. Yun ^{2,3} and Young Dae Yoon ^{1,2,*}¹*Asia Pacific Center for Theoretical Physics, Pohang, Gyeongbuk 37673, Republic of Korea*²*Department of Physics, Pohang University of Science and Technology, Pohang, Gyeongbuk 37673, Republic of Korea*³*Department of Advanced Nuclear Engineering, Pohang University of Science and Technology, Pohang, Gyeongbuk 37673, Republic of Korea* (Received 25 March 2024; revised 7 June 2024; accepted 17 August 2024; published 3 September 2024)

We show by analyzing the time evolution of canonical vorticity that spontaneous generation of magnetic fields within an initially unmagnetized, vorticity-free plasma must be achieved through the canonical battery effect. This effect generalizes well-known magnetogenesis mechanisms across different regimes such as the Biermann battery in the isotropic regime and the Weibel instability in the kinetic regime, the latter of which is further verified by particle-in-cell simulations. Using the canonical battery term, a general prediction of any configuration of the pressure tensor that allows for magnetogenesis can be established. One such configuration—a two-dimensionally localized pressure anisotropy—that does not correspond to either of the mechanisms is derived and numerically verified. The advantage of using this term in magnetogenesis analyses is discussed.

DOI: [10.1103/PhysRevResearch.6.L032052](https://doi.org/10.1103/PhysRevResearch.6.L032052)

Magnetic fields are ubiquitous in a wide range of scales and strengths from μG in interstellar media and galaxies, G around planets, stars, and black holes, to 10^{10} G around neutron stars [1–4]. Although magnetic fields play crucial roles in many physical processes in the Universe such as the formation of stars and galaxies [5,6], propagation of cosmic rays [7,8], space weather [9,10], and evolution of the Universe [11], their exact origin is still a mystery. Cosmological theories suggest that primordial magnetic fields of large coherence scales originated in the early Universe through symmetry breaking and quantum fluctuations, but the details are still under serious debate [4,8,12,13].

An alternative explanation for the origin of magnetic fields comes from plasma physics—the amplification of a seed field by turbulent dynamo [14]. Most astrophysical systems consist of rotating, conducting plasmas capable of supporting convective dynamo processes. [3,14,15]. However, initiating the dynamo requires a seed field whose self-generation is crucial but poorly understood.

Among the known mechanisms for seed-field generation, the Biermann battery effect [16] and the Weibel instability [17] are the two major theories. A Biermann battery arises due to a misalignment of density and temperature gradients [16,18], which produces a swirling motion of the plasma that generates a weak seed field. This effect has been theorized to be important in astrophysical phenomena [18,19], and observed in laser-produced plasmas [20,21].

On the other hand, the Weibel instability is a kinetic phenomenon induced by partial isotropization of an initial temperature anisotropy or equivalently counterpropagating beams [17,22]. The Weibel instability has been readily reproduced in the laboratory [23–28] and is theorized to be important in astrophysical magnetogenesis [29,30].

A seemingly disconnected theoretical framework is that associated with canonical vorticity, which is a weighted sum of fluid vorticity and magnetic field. This quantity in various forms has been used extensively in studies of magnetic reconnection [31–39] and canonical helicity [40,41]. It was recently shown that a pressure-tensor-induced effect called the “canonical battery” effect is a nonideal source of canonical vorticity and is important during magnetic reconnection [39].

In this Letter, we show that this canonical battery effect is responsible for magnetogenesis in an initially unmagnetized and vorticity-free plasma. The effect generalizes both the Biermann battery—shown trivially—and the Weibel instability—shown via particle-in-cell (PIC) simulations. Using the canonical battery term, a whole menagerie of new pressure tensor configurations can be derived that enables magnetogenesis. Two-dimensionally (2D) localized pressure anisotropy is shown to be an important mechanism which is again verified through PIC simulations. The advantage of using the canonical battery term is discussed.

Canonical battery effect. We start from the first moment of the Vlasov equation of species $\sigma = i, e$ for ions/electrons under the Lorentz force,

$$m_{\sigma} \left(\frac{\partial \mathbf{u}_{\sigma}}{\partial t} + \mathbf{u}_{\sigma} \cdot \nabla \mathbf{u}_{\sigma} \right) = q_{\sigma} (\mathbf{E} + \mathbf{u}_{\sigma} \times \mathbf{B}) - \frac{\nabla \cdot \vec{\mathbf{p}}_{\sigma}}{n_{\sigma}}, \quad (1)$$

where m_{σ} , q_{σ} , \mathbf{u}_{σ} , and n_{σ} are the species mass, charge, mean velocity, and density. \mathbf{E} and \mathbf{B} are the electric and magnetic fields, and $\vec{\mathbf{p}}_{\sigma} = m_{\sigma} \int \mathbf{v}'_{\sigma} \mathbf{v}'_{\sigma} f(\mathbf{v}_{\sigma}) d^3 \mathbf{v}_{\sigma}$ is the pressure tensor where $\mathbf{v}'_{\sigma} = \mathbf{v}_{\sigma} - \mathbf{u}_{\sigma}$ is the random part of \mathbf{v}_{σ} . We ignore

*Contact author: youngdae.yoon@apctp.org

collision terms, but viscous terms may be included as off-diagonal elements in $\vec{\mathbf{p}}_\sigma$. Taking the curl of Eq. (1), using the vector calculus identity $\nabla \times (\mathbf{V} \cdot \nabla \mathbf{V}) = -\nabla \times (\mathbf{V} \times \nabla \times \mathbf{V})$ and Faraday's law $\nabla \times \mathbf{E} = -\partial \mathbf{B} / \partial t$, and defining the vorticity $\mathbf{\Omega}_\sigma = \nabla \times \mathbf{u}_\sigma$ yields

$$m_\sigma \left[\frac{\partial \mathbf{\Omega}_\sigma}{\partial t} - \nabla \times (\mathbf{u}_\sigma \times \mathbf{\Omega}_\sigma) \right] = -q_\sigma \left[\frac{\partial \mathbf{B}}{\partial t} - \nabla \times (\mathbf{u}_\sigma \times \mathbf{B}) \right] - \nabla \times \left(\frac{\nabla \cdot \vec{\mathbf{p}}_\sigma}{n_\sigma} \right). \quad (2)$$

Now we define canonical vorticity $\mathbf{Q}_\sigma = m_\sigma \mathbf{\Omega}_\sigma + q_\sigma \mathbf{B}$ which is the curl of the canonical momentum $\mathbf{P}_\sigma = m_\sigma \mathbf{u}_\sigma + q_\sigma \mathbf{A}$ where \mathbf{A} is the magnetic vector potential. \mathbf{Q}_σ therefore represents both inertial and magnetic characteristics of the plasma species. Collecting the temporal and spatial derivatives in Eq. (2), we obtain

$$\frac{\partial \mathbf{Q}_\sigma}{\partial t} = \underbrace{\nabla \times (\mathbf{u}_\sigma \times \mathbf{Q}_\sigma)}_{\vec{\mathcal{C}}} - \nabla \times \left(\frac{\nabla \cdot \vec{\mathbf{p}}_\sigma}{n_\sigma} \right), \quad (3)$$

which is the canonical induction equation [39] that describes the time evolution of \mathbf{Q}_σ with just two terms on the right-hand side. The first term is the convective term $\vec{\mathcal{C}}$, which is isomorphic to the magnetic induction term in ideal magnetohydrodynamics (MHD) and thus signifies that \mathbf{Q}_σ is frozen into \mathbf{u}_σ . The second term is the ‘‘canonical battery’’ term $\vec{\mathcal{B}}$ which acts as a source/sink of \mathbf{Q}_σ due to the pressure tensor.

It is clear from Eq. (3) that if the plasma is unmagnetized ($\mathbf{B} = \mathbf{0}$) and vorticity free ($\mathbf{\Omega}_\sigma = \mathbf{0}$) so that $\mathbf{Q}_\sigma = \mathbf{0}$ and $\vec{\mathcal{C}} = \mathbf{0}$, the only term that can generate finite \mathbf{Q}_σ is the canonical battery term $\vec{\mathcal{B}}$. The generated \mathbf{Q}_σ cannot be entirely comprised of $\mathbf{\Omega}_\sigma$ because Ampère's law gives $-\nabla^2 \mathbf{B} = \mu_0 \nabla \times \mathbf{J} \simeq \mu_0 \sum_\sigma n_\sigma q_\sigma \mathbf{\Omega}_\sigma$, so finite $\mathbf{\Omega}_\sigma$ means finite \mathbf{B} . Therefore, spontaneous generation of \mathbf{Q}_σ and of \mathbf{B} is only possible through $\vec{\mathcal{B}}$.

To more easily understand how a canonical battery generates \mathbf{B} , let us examine a simpler system where the current is carried entirely by electrons, i.e., the electron-MHD assumption [42]. Then, $\nabla^2 \mathbf{B} = \mu_0 n_e e \mathbf{\Omega}_e$. Noting that $\sqrt{m_e / \mu_0 n_e e^2} = d_e$ is the electron skin depth, the electron canonical vorticity becomes $\mathbf{Q}_e = e(d_e^2 \nabla^2 \mathbf{B} - \mathbf{B})$ and is entirely a function of \mathbf{B} . In fact, denoting the Fourier transform by $\tilde{\mathbf{Q}}_e = \int \mathbf{Q}_e \exp(-i\mathbf{k} \cdot \mathbf{x}) d^3 \mathbf{x}$, we have

$$\mathbf{B} = -\frac{1}{2\pi e} \int \frac{\tilde{\mathbf{Q}}_e}{1 + k^2 d_e^2} \exp(i\mathbf{k} \cdot \mathbf{x}) d^3 \mathbf{k}. \quad (4)$$

Equation (4) shows that for $k^2 d_e^2 \gg 1$, \mathbf{B} is small and thus $\mathbf{Q}_e \simeq m_e \mathbf{\Omega}_\sigma$, whereas for $k^2 d_e^2 \ll 1$, $\mathbf{Q}_e \simeq -e\mathbf{B}$. For $kd_e \sim 1$, the inertial and magnetic terms contribute equally. In other words, \mathbf{B} is a ‘‘smoothed out’’ function of \mathbf{Q}_e . Therefore, the generation of \mathbf{Q}_e by the canonical battery effect necessarily generates \mathbf{B} .

To simplify the illustration of the role of the different terms in the canonical battery, let us assume $\partial / \partial z \rightarrow 0$ so the

z component of $\vec{\mathcal{B}}$ is

$$\mathcal{B}_z = \hat{z} \cdot \left[-\nabla \left(\frac{1}{n_e} \right) \times \nabla \cdot \vec{\mathbf{p}}_e \right] + \frac{1}{n_e} \left(\frac{\partial^2}{\partial y^2} - \frac{\partial^2}{\partial x^2} \right) p_{exy} + \frac{1}{n_e} \frac{\partial^2}{\partial x \partial y} (p_{exx} - p_{eyy}), \quad (5)$$

where p_{eij} is the ij component of $\vec{\mathbf{p}}_e$. Each of the three terms in Eq. (5) corresponds to different effects, as follows.

Biermann battery. The Biermann battery is simply the canonical battery with an isotropic pressure tensor. When $\vec{\mathbf{p}}_e = p_e \hat{\mathbf{I}}$, only the first term in Eq. (5) survives and becomes

$$\mathcal{B}_z = \hat{z} \cdot \left[-\nabla \left(\frac{1}{n_e} \right) \times \nabla p_e \right] = \hat{z} \cdot \left[\frac{\nabla n_e \times \nabla p_e}{n_e^2} \right], \quad (6)$$

which is exactly the Biermann battery term [16,18,21], and is the namesake of the canonical battery term.

Weibel instability. The canonical battery term also embodies the magnetic field source in the Weibel instability [17]. For simplicity, we further assume 1D ($\partial / \partial y \rightarrow 0$) and an initially uniform density ($\nabla n_e = \mathbf{0}$), then only the second term in Eq. (5) survives and becomes

$$\mathcal{B}_z = -\frac{1}{n_e} \left(\frac{\partial^2 p_{exy}}{\partial x^2} \right). \quad (7)$$

Although Weibel instability is generally attributed to pressure anisotropy $p_{eyy} > p_{exx}$, Eq. (7) explicitly shows that the mixing term p_{exy} is what generates Q_{ez} .

In order to confirm the role of \mathcal{B}_z in the Weibel instability, a 1D3V (one-dimensional in configuration space and three-dimensional in velocity space) particle-in-cell (PIC) simulation was conducted using the SMILEI code [43]. The simulation domain was $L_x = 20\pi d_e$ divided by 2048 cells, and 10^5 particles were placed per cell. Periodic boundary conditions were used, and the time step was $\Delta t = 0.0291 / \omega_{pe}$. A realistic ion-to-electron mass ratio $m_i / m_e = 1836$ was used, and the ions were initially cold. The initial electron temperatures were set as $T_{exx} = T_{ezz} = 0.001 m_e c^2$ and $T_{eyy} = 0.01 m_e c^2$, and the density was set uniformly as n_0 .

Figure 1 is a streak plot of various quantities in Eq. (3) and its constituents. It can be seen that B_z spontaneously grows due to the Weibel instability and saturates at $t\omega_{pe} \simeq 200$ [Fig. 1(a)]. The electron vorticity Ω_{ez} grows with B_z , and together they constitute $Q_{ez} = \Omega_{ez} - B_z$ in normalized units [Figs. 1(b) and 1(c)]. As expected from Eq. (4), B_z has a similar profile to Q_{ez} but without the finer sub- d_e scale structures and with the opposite sign.

Differentiating Q_{ez} with respect to time, one obtains $\partial Q_{ez} / \partial t$ [Fig. 1(d)] or the left-hand side of Eq. (3). The two terms on the right-hand side are shown in Figs. 1(e) and 1(f), which have been Gaussian filtered by seven grid points to reduce noise. It is clear that $\partial Q_{ez} / \partial t = \mathcal{B}_z$, i.e., the canonical battery effect is entirely responsible for the self-generation of Q_{ez} and of B_z .

Figure 2(a) shows the time-dependent rms value of Q_{ez} and its constituents. The exponential growth of all quantities is clear until $t\omega_{pe} \simeq 200$ with a dominance of Ω_{ez} , but after saturation Ω_{ez} and B_z are comparable. Figure 2(b) shows the rms values of the pressure tensor components. It is clear that

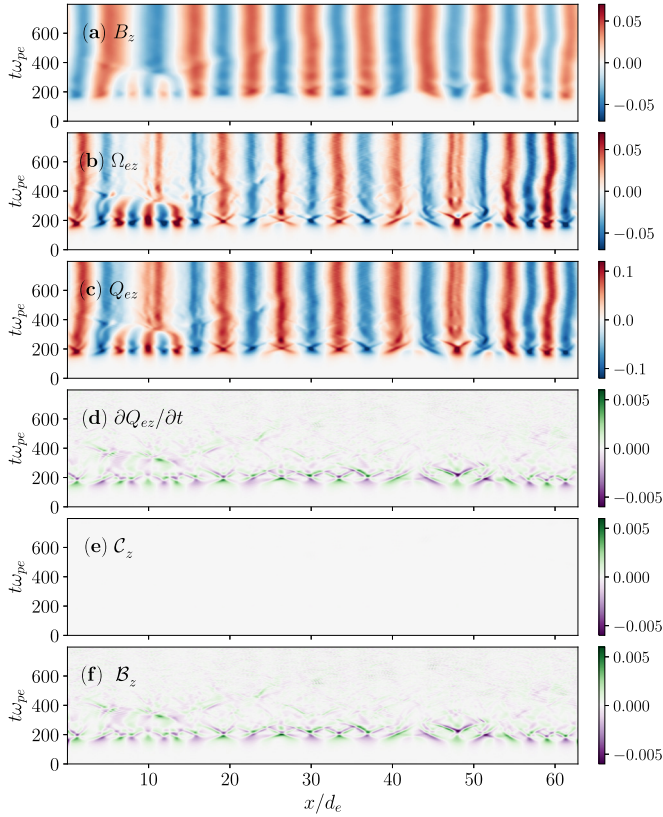


FIG. 1. Streak plot of various quantities of the z component of Eq. (3), namely (a) B_z , (b) Ω_{ez} , (c) Q_{ez} , (d) $\partial Q_{ez}/\partial t$, (e) C_z , and (f) B_z from the 1D PIC simulation. They are shown in units of (a) $m_e \omega_{pe}/e$, (b) ω_{pe} , (c) $m_e \omega_{pe}$, and (d)–(f) $m_e \omega_{pe}^2$, where $\omega_{pe} = \sqrt{n_0 e^2 / m_e \epsilon_0}$.

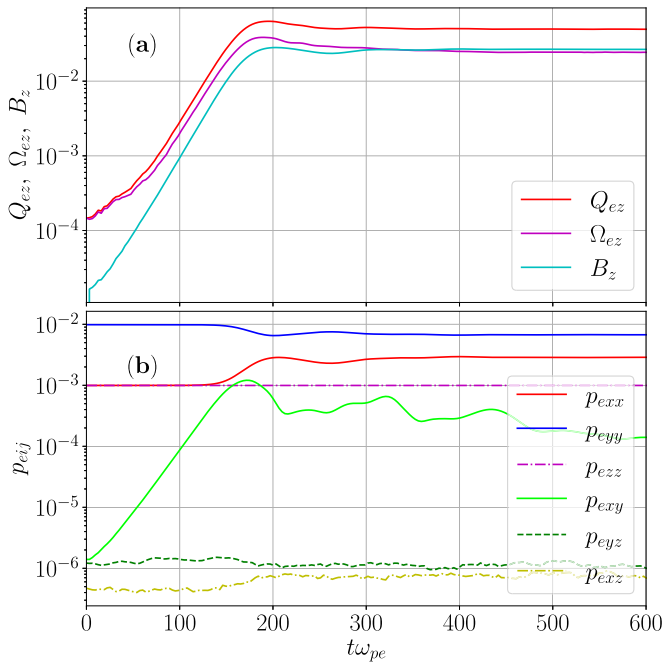


FIG. 2. Time-dependent rms values of (a) normalized Q_{ez} , Ω_{ez} , and B_z , and (b) electron pressure tensor components in units of $n_0 m_e c^2$ from the 1D simulation.

p_{exy} , which gives rise to B_z , exponentially increases as the initially high p_{eyy} is imparted to p_{exx} . After saturation, p_{exy} drops and the generation of Q_{ez} stops.

Moreover, the transition from Biermann battery to the Weibel instability around a system length scale L [44], can simply be explained by the ratio of the above two sources as follows,

$$\left| \frac{\nabla n_e \times \nabla T_e}{n_e} \right| : \frac{1}{n_e} \frac{\partial^2 p_{exy}}{\partial x^2}, \quad (8)$$

$$\frac{T_{\text{diag}}}{T_{\text{off}}} d_e^2 : L^2, \quad (9)$$

where we have assumed $\nabla^{-1} \sim L \sim L_n \sim L_T$, and T_{diag} and T_{off} are diagonal and off-diagonal components of the temperature tensor, respectively. The Weibel instability arises at d_e scales, so $\partial^2 p_{exy}/\partial x^2 \sim p_{exy}/d_e^2$. It can be seen from Fig. 2(b) that T_{diag} is around one or two orders of magnitude bigger than T_{off} and so the transition is at around $L \sim 10d_e$. Thus, the comparison between the subterms within Eq. (5) simplifies the explanation of the dependence on the length scale of the dominant field generation mechanism.

2D-localized pressure anisotropy. So far, we have established that the canonical battery effect generalizes already-known magnetogenesis mechanisms. The first and second terms in Eq. (5) are responsible for the Biermann battery and the Weibel instability, respectively. However, the canonical battery term in turn enables us to generally predict pressure tensor configurations that allow for magnetogenesis.

For instance, the third term in Eq. (5) shows that 2D-localized pressure anisotropy can also directly generate magnetic fields, which is different from the Weibel instability that involves only the mixing term p_{exy} . In particular, if the initial localized anisotropy is of the form $p_{exx} - p_{eyy} \sim \exp[-(x^2 + y^2)/\sigma^2]$ with uniform density, then only the third term in Eq. (5) survives and has the dependence

$$B_z \sim xy \exp\left(-\frac{x^2 + y^2}{\sigma^2}\right), \quad (10)$$

which means that a quadrupole magnetic field will be locally generated.

To verify these predictions, a 2D3V PIC simulation was conducted in the domain $(L_x, L_y) = (10, 10)d_e$ divided into 2048 cells in each direction. Two hundred particles were placed per cell and the time step was $\Delta t = 3.28 \times 10^{-3}/\omega_{pe}$. The electromagnetic (EM) boundary conditions were Silver-Müller, and particles were removed upon boundary exit. The initial electron temperatures were $T_{eyy} = T_{ezz} = 10^{-4} m_e c^2$ and $T_{exx} = T_{eyy} + 0.04 m_e c^2 \exp[-[(x - x_0)^2 + (y - y_0)^2]/\sigma^2]$ where $\sigma = \sqrt{0.5}d_e$ and $x_0 = y_0 = 5d_e$ with uniform density n_0 . The ion temperatures were set uniformly to $10^{-4} m_e c^2$ and $m_i/m_e = 1836$.

Figure 3 shows streak plots of various quantities from the 2D simulation. All quantities have been Gaussian filtered by ten grid points. A quadrupole B_z is indeed generated [Fig. 3(a)] as predicted from Eq. (10). A quadrupole Ω_{ez} is also generated, which combines with B_z to yield Q_{ez} [Figs. 3(b) and 3(c)]. The sign of the vorticity corresponds to inflow in the $\pm y$ directions and outflow in the $\pm x$ directions.

The magnetic field strength is comparable to that of the Weibel instability [Fig. 1(a)]. For a plasma density of

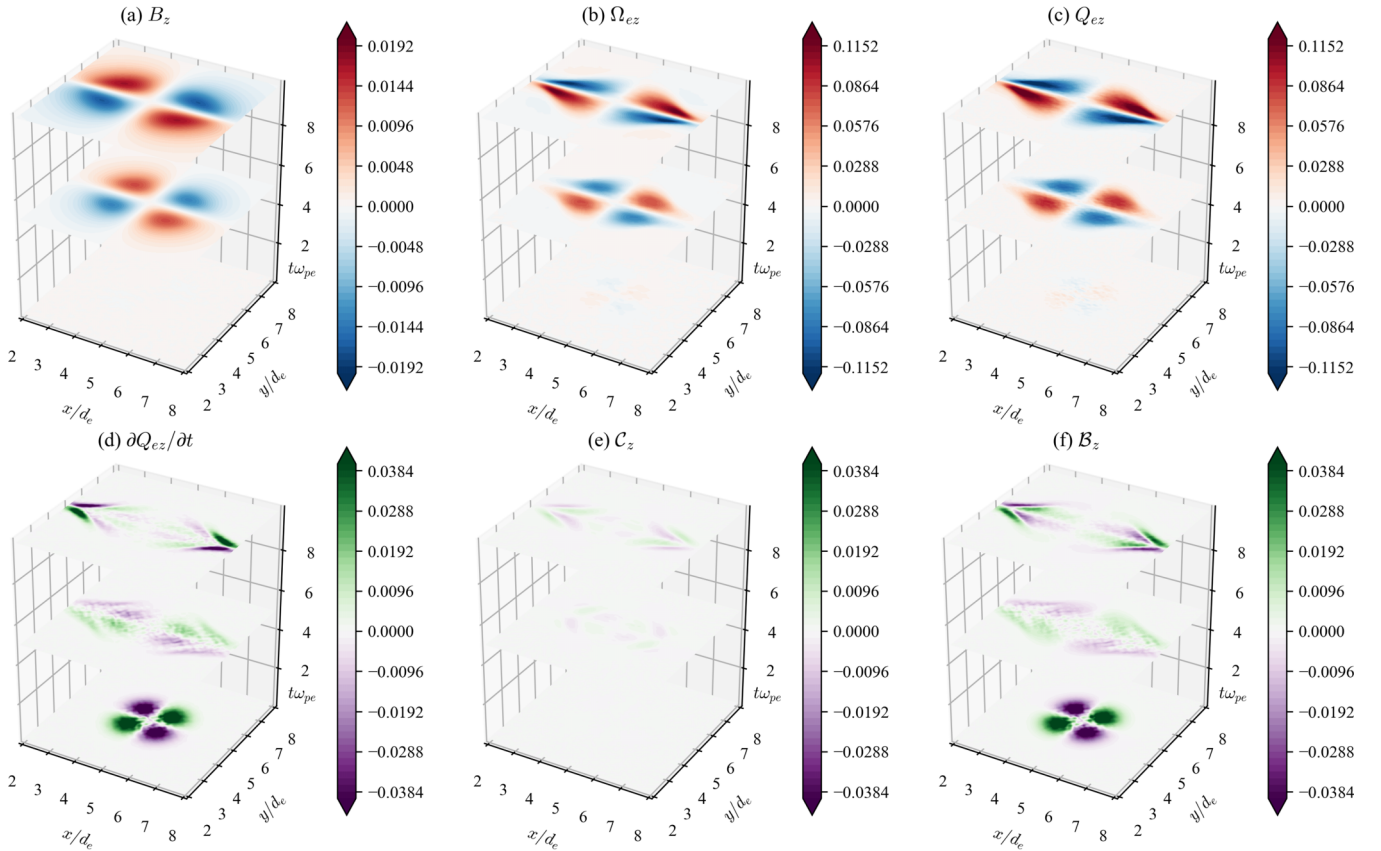


FIG. 3. Streak plots of (a) B_z , (b) Ω_{ez} , (c) Q_{ez} , (d) $\partial Q_{ez}/\partial t$, (e) C_z , and (f) B_z from the 2D PIC simulation. The units are the same as in Fig. 1. The three slices in each panel correspond to $t\omega_{pe} = 0.19, 5.02, 9.94$.

$n_0 = 10^{19} \text{ cm}^{-3}$ as is typically generated from laser-matter interactions [28], the strength corresponds to 20 T.

Figure 3(d) shows $\partial Q_{ez}/\partial t$, calculated with a backward difference scheme. Note that in this case the data were saved at sparse time intervals and so the calculation of $\partial Q_{ez}/\partial t$ is relatively inaccurate. Figure 3(f) shows B_z which reasonably reproduces $\partial Q_{ez}/\partial t$, again confirming the role of the canonical battery effect. B_z initially generates quadrupole structures and then propagates in the $\pm x$ directions. Figure 3(e) shows that C_z is also generated but is relatively weak.

Figure 4 shows the maximum values of various quantities in the simulation. It can be seen that the B_z grows and saturates within $\sim 2/\omega_{pe}$, but p_{exy} does not change until later, demonstrating that the third term in Eq. (5) is generating B_z . In fact, the first and second terms in Eq. (5) are found to be negligible in the simulation.

On top of the setups presented here, a whole menagerie of pressure tensor configurations that lead to magnetogenesis can be generally predicted with the canonical battery terms. For example, if a strong density inhomogeneity ($\nabla n_e \neq 0$) and pressure anisotropy coexist, the first term in Eq. (5) does *not* approximate to the Biermann battery term and creates much stronger magnetic fields (see Appendix for further analyses in this case). This configuration should be important in laser experiments with localized densities [46,47]. Similarly, there can be multiple structures of Q_{ez} from all possible combinations of the source terms in Eq. (5). Magnetogenesis by the ion canonical battery effect should also be possible.

Discussion. The canonical battery effect due to the pressure tensor anisotropy is important in many magnetic-field-generating scenarios. In fact, the proposed

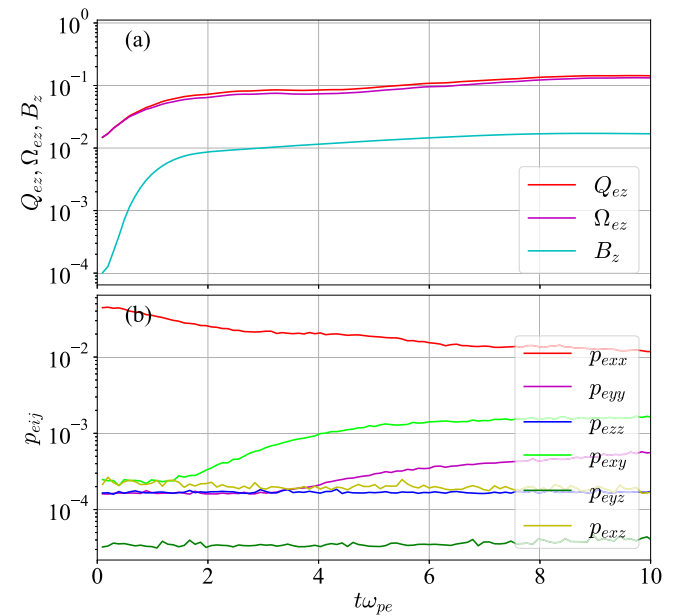


FIG. 4. Time-dependent maximum values of (a) normalized Q_{ez} , Ω_{ez} , and B_z , and (b) electron pressure tensor components in units of $n_0 m_e c^2$ from the 2D simulation.

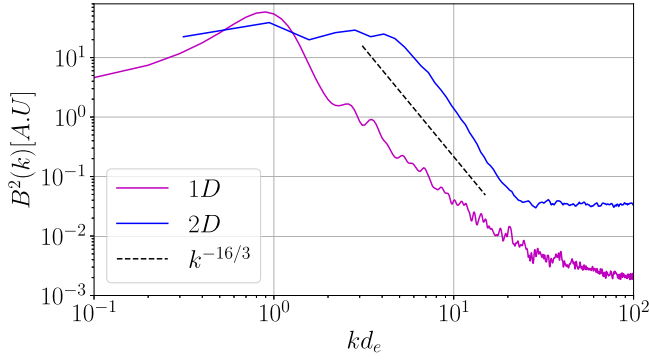


FIG. 5. Fourier spectrum of B^2 in arbitrary units after saturation in both the 1D and 2D simulations. The dashed line shows a power law of $k^{-16/3}$, which is predicted by gyrokinetic theory of turbulence [45].

kinetic theory and simulation shows that arbitrary density and temperature gradients lead to localized anisotropies which leads to magnetic-field generation on top of the well-known Biermann battery effect [16] and the Weibel instability [17]. In experiments that investigate magnetogenesis and related phenomena through focused laser beams, such localized anisotropy is usually inevitable and should be consequential [46–48]. Schoeffler *et al.* [44] showed that the relative importance of the Biermann effect to the Weibel instability depends on the length scale of the source. As shown in Eq. (9), a scaling comparison between the subterms in the canonical battery term can simply explain such dependence on the dominant sources.

Different generation mechanisms engender different energy spectra, which may influence subsequent dynamo amplification. Figure 5 shows that the dominant wave number in the Weibel instability is around $kd_e \lesssim 1$, whereas for the new 2D case it extends to $kd_e > 1$. This fact is also manifested in Fig. 2(a) where $\Omega_{ey} \simeq B_y$ and Fig. 4(a) where $\Omega_{ez} \gg B_z$. They also have different growth rates; the present 2D case has a larger growth rate than the Weibel instability.

Although we focus on seed-field generation here, Eq. 3 also allows us to distinguish between seed-field generation and dynamo-driven amplification. The former should be associated with the canonical battery term, whereas the latter with the convective term. Therefore, by examining the interplay between the two terms, one can identify the progression of magnetic fields from microscales to macroscales. Such transitions have been gaining recent attention [30,49] and are worth exploring in the canonical vorticity framework, especially because the merging or breaking of Weibel-induced filaments involve reconnection which is controlled by both convective and battery terms [35,36,39]. Even after the relaxation of the canonical battery effect and of the system to MHD scales, stochasticity may induce further dynamo effects [50,51]. Studies of such effects requires considerations in 3D, which will engender more terms in Eq. (5).

A simple scaling comparison of the convective and battery terms in Eq. (3) ($|\mathbf{u}_e \times \mathbf{Q}_e| : |\nabla \cdot \vec{p}_e/n_e|$) can be conducted to estimate the length scale at which this transition occurs, assuming that the convective term becomes the dynamo term when $|\mathbf{u}_e| \sim v_A$ (Alfvén velocity) and $\mathbf{Q}_e \sim \mathbf{B}$. Further

writing $\nabla \sim L^{-1}$, one can show that the battery effect is dominant over amplification for characteristic lengths up to $L \approx \beta_e d_i/2$, where $\beta_e = 2\mu_0 p_e/B^2$ is the electron plasma beta and $d_i = \sqrt{m_i/\mu_0 n_e}$ is the ion skin depth.

Moreover, quadrupole field generation by the localized pressure anisotropy also has implications for magnetic reconnection [52] and flux rope generation [53], suggesting that the proposed model may be used for detailed studies of magnetic reconnection characteristics involved in the flux rope dynamics in astrophysical plasmas. Note that \mathbf{Q}_e flux can be a conserved quantity while \mathbf{B} flux is not. A possibly more astrophysically relevant scenario is magnetogenesis in, e.g., supernovae, shocks, and/or pair plasmas, which requires considerations of relativistic effects [54–56]. Our preliminary investigations show that relativistic effects are manifested as single additional term in Eq. (3).

In summary, we have found different magnetogenesis mechanisms by analyzing the canonical battery effect which is responsible for the spontaneous generation of canonical vorticity. The effect also generalizes popular mechanisms such as Biermann battery and Weibel instability, and generally predicts pressure tensor configurations that can generate seed magnetic fields. Implications for future magnetogenesis analyses were also discussed.

Acknowledgments. This work was supported by an appointment to the JRG Program at the APCTP through the Science and Technology Promotion Fund and Lottery Fund of the Korean government, and also by the Korean Local Governments—Gyeongsangbuk-do Province and Pohang City. This work was also supported by the National Research Foundation of Korea under Grant No. RS-2023-00281272. The computations presented here were conducted on the KAIROS supercomputing cluster at the Korean Institute of Fusion Energy, and on the APCTP computing server.

Appendix: additional cases. Consider an initially nonuniform density $n_e = n_0 \exp\{-[(x - x_0)^2 + (y - y_0)^2]/2\sigma^2\}$ coexisting with the 2D-localized pressure anisotropy shown in Fig. 3. In this case, the dominant term of the battery, in addition to Eq. (10), is

$$\mathcal{B}_z \sim \left(\frac{\partial}{\partial y} \frac{1}{n_e} \right) \left(\frac{\partial p_{exx}}{\partial x} \right), \quad (\text{A1})$$

which has the dependence $\propto -xy$ and so opposes the original term [Eq. (10)]. Therefore, the quadrupole magnetic field generation is expected to be reduced.

Figure 6 shows the corresponding simulation result of B_z at $t\omega_{pe} = 5$, which is compared with the middle slice in Fig. 3(a), that has a maximum B_z amplitude of 0.014. By comparison, the above figure shows that the maximum of the generated B_z is only around 0.004, which is a reduction that is accurately predicted by Eq. (A1).

Consider another case with the same initial nonuniform $n_e = n_0 \exp\{-[(x - x_0)^2 + (y - y_0)^2]/2\sigma^2\}$ but with nonlocalized electron temperatures anisotropy of $T_{eyy} = T_{ezz} = 10^{-4} m_e c^2$ and $T_{exx} = 0.04 m_e c^2$. All other parameters remain unchanged. In this case the additional dominant term, assuming $p_{eij} = n_e T_{eij}$, is

$$\mathcal{B}_z \sim T_{exx} \left(\frac{\partial}{\partial y} \frac{1}{n_e} \right) \left(\frac{\partial n_e}{\partial x} \right), \quad (\text{A2})$$

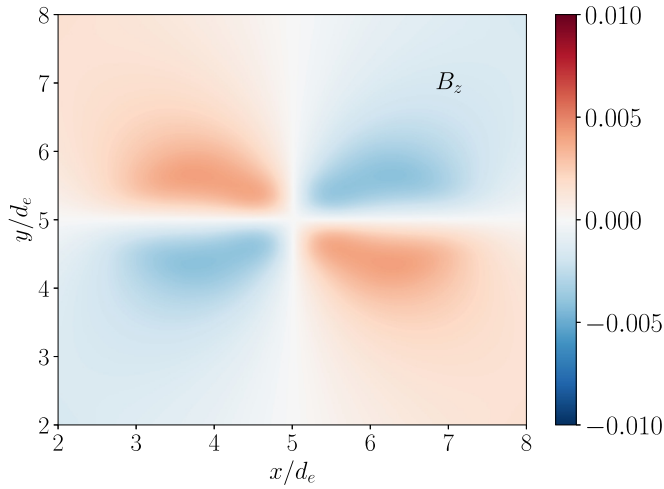


FIG. 6. Strength of quadrupole B_z on the xy plane at $t\omega_{pe} = 5$ for the localized both n_e and T_{eij} case.

which also has the dependence $\propto -xy$ and so opposes the original term [Eq. (10)]. However, Eq. (A1) involves gradients in both n_e and T_{exx} and so its magnitude should be stronger than Eq. (A2), and so the reduction given by Eq. (A2) should be weaker than that of Eq. (A1).

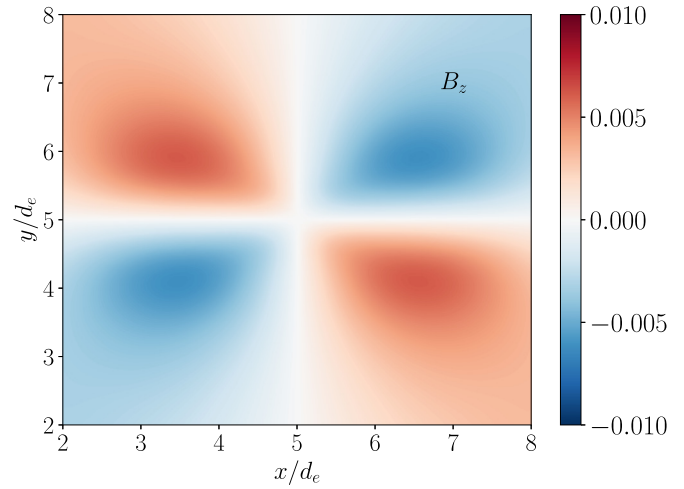


FIG. 7. Strength of quadrupole B_z on the xy plane at $t\omega_{pe} = 5$ for the localized n_e and nonlocalized T_{eij} case.

Figure 7 shows the corresponding B_z at the $t\omega_{pe} = 5$ and compared with the middle slice of Figs. 3(a) and 6. By comparison, Fig. 7 shows that the magnitude of the generated B_z is around 0.007, which is also a reduction but that is indeed weaker than in the previous case.

-
- [1] E. N. Parker, *Cosmical Magnetic Fields: Their Origin and Their Activity* (Clarendon Press, Oxford, UK, 1979).
- [2] A. Bonafede, L. Feretti, M. Murgia, F. Govoni, G. Giovannini, D. Dallacasa, K. Dolag, and G. B. Taylor, The coma cluster magnetic field from Faraday rotation measures, *Astron. Astrophys.* **513**, A30 (2010).
- [3] A. Brandenburg and K. Subramanian, Astrophysical magnetic fields and nonlinear dynamo theory, *Phys. Rep.* **417**, 1 (2005).
- [4] T. Vachaspati, Progress on cosmological magnetic fields, *Rep. Prog. Phys.* **84**, 074901 (2021).
- [5] M. Vogelsberger, F. Marinacci, P. Torrey, and E. Puchwein, Cosmological simulations of galaxy formation, *Nat. Rev. Phys.* **2**, 42 (2020).
- [6] H. Li, O. Y. Gnedin, and N. Y. Gnedin, Star cluster formation in cosmological simulations. II. Effects of star formation efficiency and stellar feedback, *Astrophys. J.* **861**, 107 (2018).
- [7] G. Bertone, C. Isola, M. Lemoine, and G. Sigl, Ultrahigh energy heavy nuclei propagation in extragalactic magnetic fields, *Phys. Rev. D* **66**, 103003 (2002).
- [8] A. Neronov and I. Vovk, Evidence for strong extragalactic magnetic fields from Fermi observations of TeV blazars, *Science* **328**, 73 (2010).
- [9] J. M. Griebmeier, F. Tabataba-Vakili, A. Stadelmann, J. L. Grenfell, and D. Atri, Galactic cosmic rays on extrasolar earth-like planets: I. Cosmic ray flux, *Astron. Astrophys.* **581**, A44 (2015).
- [10] I. P. Pakhotin, I. R. Mann, K. Xie, J. K. Burchill, and D. J. Knudsen, Northern preference for terrestrial electromagnetic energy input from space weather, *Nat. Commun.* **12**, 199 (2021).
- [11] M. S. Turner and L. M. Widrow, Inflation-produced, large-scale magnetic fields, *Phys. Rev. D* **37**, 2743 (1988).
- [12] K. Jedamzik and A. Saveliev, Stringent limit on primordial magnetic fields from the cosmic microwave background radiation, *Phys. Rev. Lett.* **123**, 021301 (2019).
- [13] K. Jedamzik and L. Pogosian, Relieving the Hubble tension with primordial magnetic fields, *Phys. Rev. Lett.* **125**, 181302 (2020).
- [14] A. Brandenburg, D. Sokoloff, and K. Subramanian, Current status of turbulent dynamo theory: From large-scale to small-scale dynamos, *Space Sci. Rev.* **169**, 123 (2012).
- [15] J. Mason, L. Malyshkin, S. Boldyrev, and F. Cattaneo, Magnetic dynamo action in random flows with zero and finite correlation times, *Astrophys. J.* **730**, 86 (2011).
- [16] A. Schlüter, Über den ursprung der magnetfelder auf sternnen und im interstellaren raum, *Z. Naturforsch. A* **5**, 65 (1950).
- [17] E. S. Weibel, Spontaneously growing transverse waves in a plasma due to an anisotropic velocity distribution, *Phys. Rev. Lett.* **2**, 83 (1959).
- [18] R. M. Kulsrud, R. Cen, J. P. Ostriker, and D. Ryu, The protogalactic origin for cosmic magnetic fields, *Astrophys. J.* **480**, 481 (1997).
- [19] N. Y. Gnedin, A. Ferrara, and E. G. Zweibel, Generation of the primordial magnetic fields during cosmological reionization, *Astrophys. J.* **539**, 505 (2000).
- [20] P. M. Nilson, L. Willingale, M. C. Kaluza, C. Kamperidis, S. Minardi, M. S. Wei, P. Fernandes, M. Notley, S. Bandyopadhyay, M. Sherlock, R. J. Kingham, M. Tatarakis, Z. Najmudin, W. Rozmus, R. G. Evans, M. G. Haines, A. E. Dangor, and K. Krushelnick, Magnetic reconnection and

- plasma dynamics in two-beam laser-solid interactions, *Phys. Rev. Lett.* **97**, 255001 (2006).
- [21] J. Matteucci, W. Fox, A. Bhattacharjee, D. B. Schaeffer, C. Moissard, K. Germaschewski, G. Fiksel, and S. X. Hu, Biermann-battery-mediated magnetic reconnection in 3D colliding plasmas, *Phys. Rev. Lett.* **121**, 095001 (2018).
- [22] A. Grassi, M. Grech, F. Amiranoff, F. Pegoraro, A. Macchi, and C. Riconda, Electron Weibel instability in relativistic counterstreaming plasmas with flow-aligned external magnetic fields, *Phys. Rev. E* **95**, 023203 (2017).
- [23] J. A. Stamper, K. Papadopoulos, R. N. Sudan, S. O. Dean, E. A. McLean, and J. M. Dawson, Spontaneous magnetic fields in laser-produced plasmas, *Phys. Rev. Lett.* **26**, 1012 (1971).
- [24] N. L. Kugland, D. D. Ryutov, P. Y. Chang, R. P. Drake, G. Fiksel, D. H. Froula, S. H. Glenzer, G. Gregori, M. Grosskopf, M. Koenig, Y. Kuramitsu, C. Kuranz, M. C. Levy, E. Liang, J. Meinecke, F. Miniati, T. Morita, A. Pelka, C. Plechaty, R. Presura *et al.*, Self-organized electromagnetic field structures in laser-produced counter-streaming plasmas, *Nat. Phys.* **8**, 809 (2012).
- [25] J. Zhong, Y. Li, X. Wang, J. Wang, Q. Dong, C. Xiao, S. Wang, X. Liu, L. Zhang, L. An, F. Wang, J. Zhu, Y. Gu, X. He, G. Zhao, and J. Zhang, Modelling loop-top x-ray source and reconnection outflows in solar flares with intense lasers, *Nat. Phys.* **6**, 984 (2010).
- [26] S. Mondal, V. Narayanan, W. J. Ding, A. D. Lad, B. Hao, S. Ahmad, W. M. Wang, Z. M. Sheng, S. Sengupta, P. Kaw, A. Das, and G. R. Kumar, Direct observation of turbulent magnetic fields in hot, dense laser produced plasmas, *Proc. Natl. Acad. Sci. USA* **109**, 8011 (2012).
- [27] W. Fox, G. Fiksel, A. Bhattacharjee, P.-Y. Chang, K. Germaschewski, S. X. Hu, and P. M. Nilson, Filamentation instability of counterstreaming laser-driven plasmas, *Phys. Rev. Lett.* **111**, 225002 (2013).
- [28] C. M. Huntington, F. Fiuza, J. S. Ross, A. B. Zylstra, R. P. Drake, D. H. Froula, G. Gregori, N. L. Kugland, C. C. Kuranz, M. C. Levy, C. K. Li, J. Meinecke, T. Morita, R. Petrasso, C. Plechaty, B. A. Remington, D. D. Ryutov, Y. Sakawa, A. Spitkovsky, H. Takabe *et al.*, Observation of magnetic field generation via the Weibel instability in interpenetrating plasma flows, *Nat. Phys.* **11**, 173 (2015).
- [29] F. Pucci, M. Viviani, F. Valentini, G. Lapenta, W. H. Matthaeus, and S. Servidio, Turbulent magnetogenesis in a collisionless plasma, *Astrophys. J. Lett.* **922**, L18 (2021).
- [30] M. Zhou, V. Zhdankin, M. W. Kunz, N. F. Loureiro, and D. A. Uzdensky, Magnetogenesis in a collisionless plasma: From Weibel instability to turbulent dynamo, *Astrophys. J.* **960**, L2 (2024).
- [31] S. V. Bulanov, F. Pegoraro, and A. S. Sakharov, Magnetic reconnection in electron magnetohydrodynamics, *Phys. Fluids B* **4**, 2499 (1992).
- [32] D. Biskamp, E. Schwarz, and J. F. Drake, Two-fluid theory of collisionless magnetic reconnection, *Phys. Plasmas* **4**, 1002 (1997).
- [33] E. Cafaro, D. Grasso, F. Pegoraro, F. Porcelli, and A. Saluzzi, Invariants and geometric structures in nonlinear Hamiltonian magnetic reconnection, *Phys. Rev. Lett.* **80**, 4430 (1998).
- [34] D. Grasso, F. Califano, F. Pegoraro, and F. Porcelli, Phase mixing and island saturation in Hamiltonian reconnection, *Phys. Rev. Lett.* **86**, 5051 (2001).
- [35] Y. D. Yoon and P. M. Bellan, A generalized two-fluid picture of non-driven collisionless reconnection and its relation to whistler waves, *Phys. Plasmas* **24**, 052114 (2017).
- [36] Y. D. Yoon and P. M. Bellan, An intuitive two-fluid picture of spontaneous 2D collisionless magnetic reconnection and whistler wave generation, *Phys. Plasmas* **25**, 055704 (2018).
- [37] Y. D. Yoon and P. M. Bellan, Fast ion heating in transient collisionless magnetic reconnection via an intrinsic stochastic mechanism, *Astrophys. J. Lett.* **868**, L31 (2018).
- [38] S. M. Mahajan and F. A. Asenjo, General connected and reconnected fields in plasmas, *Phys. Plasmas* **25**, 022116 (2018).
- [39] Y. D. Yoon and P. M. Bellan, The electron canonical battery effect in magnetic reconnection: Completion of the electron canonical vorticity framework, *Phys. Plasmas* **26**, 100702 (2019).
- [40] S. You, A field theory approach to the evolution of canonical helicity and energy, *Phys. Plasmas* **23**, 072108 (2016).
- [41] J. V. D. Linden, J. Sears, T. Intrator, and S. You, Measurements of the canonical helicity of a gyrating kink, *Phys. Rev. Lett.* **121**, 035001 (2018).
- [42] A. V. Gordeev, A. S. Kingsep, and L. I. Rudakov, Electron magnetohydrodynamics, *Phys. Rep.* **243**, 215 (1994).
- [43] J. Derouillat, A. Beck, F. Pérez, T. Vinci, M. Chiaramello, A. Grassi, M. Flé, G. Bouchard, I. Plotnikov, N. Aunai, J. Dargent, C. Riconda, and M. Grech, SMILEI: A collaborative, open-source, multi-purpose particle-in-cell code for plasma simulation, *Comput. Phys. Commun.* **222**, 351 (2018).
- [44] K. M. Schoeffler, N. F. Loureiro, R. A. Fonseca, and L. O. Silva, Magnetic-field generation and amplification in an expanding plasma, *Phys. Rev. Lett.* **112**, 175001 (2014).
- [45] A. A. Schekochihin, S. C. Cowley, W. Dorland, G. W. Hammett, G. G. Howes, E. Quataert, and T. Tatsuno, Astrophysical gyrokinetics: Kinetic and fluid turbulent cascades in magnetized weakly collisional plasmas, *Astrophys. J. Suppl. Ser.* **182**, 310 (2009).
- [46] Y. Kuramitsu, Y. Sakawa, T. Morita, S. Dono, H. Aoki, H. Tanji, C. D. Gregory, J. N. Waugh, B. Loupias, M. Koenig, N. Woolsey, T. Ide, T. Sano, and H. Takabe, Formation of density inhomogeneity in laser produced plasmas for a test bed of magnetic field amplification in supernova remnants, *Astrophys. Space Sci.* **336**, 269 (2011).
- [47] S. Jinno, M. Kanasaki, T. Asai, R. Matsui, A. S. Pirozhkov, K. Ogura, A. Sagisaka, Y. Miyasaka, N. Nakanii, M. Kando, N. Kitagawa, K. Morishima, S. Kodaira, Y. Kishimoto, T. Yamauchi, M. Uesaka, H. Kiriyama, and Y. Fukuda, Laser-driven multi-MeV high-purity proton acceleration via anisotropic ambipolar expansion of micron-scale hydrogen clusters, *Sci. Rep.* **12**, 16753 (2022).
- [48] C. Zhang, C.-K. Huang, K. A. Marsh, C. E. Clayton, W. B. Mori, and C. Joshi, Ultrafast optical field-ionized gases—A laboratory platform for studying kinetic plasma instabilities, *Sci. Adv.* **5**, eaax4545 (2019).
- [49] L. Sironi, L. Comisso, and R. Golant, Generation of near-equipartition magnetic fields in turbulent collisionless plasmas, *Phys. Rev. Lett.* **131**, 055201 (2023).
- [50] G. L. Eyink, A. Lazarian, and E. T. Vishniac, Fast magnetic reconnection and spontaneous stochasticity, *Astrophys. J.* **743**, 51 (2011).
- [51] G. L. Eyink, Stochastic flux freezing and magnetic dynamo, *Phys. Rev. E* **83**, 056405 (2011).

- [52] J. Egedal, A. Le, and W. Daughton, A review of pressure anisotropy caused by electron trapping in collisionless plasma, and its implications for magnetic reconnection, *Phys. Plasmas* **20**, 061201 (2013).
- [53] S. Kumar, A. Prasad, S. S. Nayak, S. Agarwal, and R. Bhattacharyya, Magnetohydrodynamics simulation of magnetic flux rope formation in a quadrupolar magnetic field configuration, *Plasma Phys. Controlled Fusion* **65**, 085008 (2023).
- [54] A. Bohdan, M. Pohl, J. Niemiec, P. J. Morris, Y. Matsumoto, T. Amano, M. Hoshino, and A. Sulaiman, Magnetic field amplification by the Weibel instability at planetary and astrophysical shocks with high Mach number, *Phys. Rev. Lett.* **126**, 095101 (2021).
- [55] M. Iwamoto, T. Amano, M. Hoshino, Y. Matsumoto, J. Niemiec, A. Ligorini, O. Kobzar, and M. Pohl, Precursor wave amplification by ion-electron coupling through wake-field in relativistic shocks, *Astrophys. J. Lett.* **883**, L35 (2019).
- [56] M. Iwamoto, Y. Matsumoto, T. Amano, S. Matsukiyo, and M. Hoshino, Linearly polarized coherent emission from relativistic magnetized ion-electron shocks, *Phys. Rev. Lett.* **132**, 035201 (2024).